International Journal of Solids and Structures 48 (2011) 1778–1790

Contents lists available at ScienceDirect

International Journal of Solids and Structures

journal homepage: www.elsevier.com/locate/ijsolstr

An inclined surface crack subject to biaxial loading

V.N. Shlyannikov *, A.V. Tumanov

Research Center for Power Engineering Problems of the Russian Academy of Sciences, Lobachevsky Street, 2/31, P.O. Box 190, Kazan 420111, Russia

ARTICLE INFO

Article history:
Received 13 November 2010
Received in revised form 18 January 2011
Available online 2 March 2011

Keywords:
Inclined semi-elliptical crack
Load biaxiality
Mode mixity
Crack tip singularity
Crack growth direction

ABSTRACT

The elastic–plastic stress fields and mode mixity parameters for semi-elliptical surface cracks on biaxial loaded plates have been investigated using detailed three-dimensional finite element calculations. Different degrees of mode mixity are given by combinations of the far-field stress level, biaxial stress ratio and inclined crack angle. These analyses were performed for different surface flaw geometries to study the combined load biaxiality and mode mixity effects on the crack-front stress fields and the size and shape of the plastic zones. It is clear from considering the local stress distributions along the crack front that the elastic crack tip singularities have been derived for several particular cases of mixed mode biaxial loading. By theoretical analysis, the new formulae have been introduced for both the elastic and plastic mode-mixity parameters, accounting for ratios between the I/II, II/III and III/I modes. Particular attention was paid to the strong variations of the mode-mixity parameters along the semi-elliptical surface crack front. The mixed-mode behavior of the crack growth direction angle along the semi-elliptical crack front for different combinations of biaxial loading and inclination crack angles was also determined. It was done using methods based on the maximum tangential stress and the strain energy density criteria.

Published by Elsevier Ltd.

1. Introduction

A literature review shows that (Dalle Donne, 1999; Aoki et al., 1987) there are two competing fracture mechanisms in a ductile material under mixed-mode loading that are operative near the sharpened and blunted site of the notch, respectively. Moreover, the mixed-mode ratio will certainly have an effect, and a transition at the site of the crack initiation may be observed with a change of the loading conditions. The dominant mechanism determines the stable crack growth direction. The principal feature of such crack growth is that the stable crack propagates either as being dominated by a tensile crack fracture mechanism in approximately the direction normal to the maximum tangential stresses, or as being dominated by a shear crack fracture mechanism in the maximum strain direction.

The mode mixity has also been proven to be an important parameter in characterizing the near tip elastic–plastic fields of 2D and 3D crack problems. Li et al. (2004) established a criterion to study the competition between the tensile fracture and the shear fracture in the frame of Ritchie–Knott–Rice (RKR) conception (Ritchie et al., 1973). Based on the generalization by Shih (1974), on the HRR-solution and on the knowledge of the mixity parameter M_P, the RKR-based criterion is transformed into a J–M_P criterion. This criterion is given as a function of the mixity parameter M_P and the strain hardening exponent n of the material. When the crack grows in accordance with the cleavage fracture mechanism in elastic solids, the mixed-mode crack behavior can be described by either the elastic stress intensity factors K_I and K_{II} or the elastic-mixity parameters M_E. Moreover, the criteria used to assess the crack growth direction angle for both tensile and shear crack must be also scaled by M_E or M_P.

All of the considered criteria are only applicable when a highly accurate evaluation of the mixity parameters M_E or M_P has been given. Therefore, it is physically more reasonable to establish mixed-mode fracture criteria on the basis of the J–M_E and J–M_P annuli. In these criteria, the elastic M_E and the plastic M_P are both governing parameters of the mixed-mode crack behavior. Even if some attempts have been made recently, there are currently no results available to provide the critical applied mixed-mode ratio characterizing the usual change in the fracture mode.

All of the above-mentioned (both analytical and numerical) analyses of the effects of the dominant fracture mechanism during mixed-mode loading have focused only on through thickness crack type (Shlyannikov, 2010). A similar investigation of inclined surface cracks in elastic–plastic solids has not been carried out. Only a few works related to 3D-analysis of fracture criteria and parameters behavior have been presented in the literature (Ayhan, 2004; English et al., 2010; Miura and Takahashi, 2010; Wang, 2006; Burdekin and Xu, 2003; Zhao et al., 2007).

Surface flaws are typical damage to different types of engineering structures. The assessment of changes in both the form and the size of the surface cracks during propagation is an essential element for the prediction of the structural integrity of biaxially

* Corresponding author. Tel.: +7 843 231 90 20.
E-mail address: shlyannikov@mail.ru (V.N. Shlyannikov).

0020-7683/$ - see front matter Published by Elsevier Ltd.
doi:10.1016/j.ijsolstr.2011.02.024

loaded engineering structures, such as pressured vessels and pipelines in the presence of initial and accumulated operation damages. Frequently in practice, inclined cracks are encountered and accurate assessment of the fracture resistance under monotonic loading or the remaining fatigue life for such problems requires one to account for the geometrically induced mode mixity, i.e., the non-normal crack in the loading direction. Therefore three-dimensional solutions obtained for biaxially loaded plates containing inclined surface flaws can generally be very useful in assessing the fracture conditions in the given problem of interest.

In their study, Tai et al. (2010) considered the effects of *T*-stress, in addition to K_I, K_{II} and K_{III} with respect to predicting the fracture initiation angle for 3D surface mixed-mode cracks. They have shown, on the basis of the maximum tangential stress criterion, that for linear elastic materials, a negative T increases the apparent fracture toughness, whereas a positive one decreases it.

Fig. 1 illustrates an inclined, semi-elliptical surface crack in a plate loaded by uniform biaxial loads. Load biaxiality is given by the ratio of the nominal stresses $\eta = \sigma^n_{xx}/\sigma^n_{yy}$. In this figure, a is the crack depth in the plate thickness direction and $2c$ is the crack length in the plate width/height direction, and they are measured in the inclined crack plane *A–A*. The crack plane *A–A* is rotated with respect to the global *OZ* axis by α (Fig. 1). The angle of inclination, α, is measured from a plane parallel to the global *X–Z* plane, i.e., α is the angle between the crack plane *A–A* and the global *X–Z* plane. It should be noted that the position angle along either the crack front, or the parametric angle φ of a semi-ellipse goes from 0° to 180° in the plots for this type of surface flaw and this angle is measured from the upper free surface, i.e., $\varphi = 0°$. The size of the plate containing the inclined surface flaw is taken as $w/c \gg 1$ and $t/a \gg 1$ in all of the cases considered here.

The surface flaw in Fig. 1 undergoes mixed-mode fracture conditions having all three components of stress intensity factors, i.e., mode I, mode II and mode III. Although the remote loading takes place under normal pressure loads, an abnormal orientation of the crack relative to the loading direction causes the mode mixity. Different degrees of mixed modes are given by the combinations of the crack plane position angle α and the load biaxiality η. For instance, a tensile load (or pure mode I) corresponds to $\alpha = 90°$ for any η and φ, however, for $\alpha = 45°$, $\eta = -1$ at $\varphi = 0°$ occurs in pure mode II on the free surface of the plate. Similarly, the same values $\alpha = 45°$, $\eta = -1$ at $\varphi = 90°$ in the deepest point of the crack front realize pure mode III. There is no geometrical symmetry in this problem.

The main objective of the present work is to study the influence of the aspect ratio of a semi-elliptical surface flaw, biaxial loading and an initial crack angle on the elastic–plastic stress–strain fields. This is done for both elastic M_E and plastic M_P mode-mixity parameter distributions and the crack growth direction angle behavior for a surface crack is subjected to combined loading in modes I, II and III. The present investigation is carried out within the framework of extensive 3D finite element analysis and under all three fracture mode (combining mode I, mode II and mode III) conditions.

2. Computational procedures

2.1. Coordinate systems

Fig. 1 shows a schematic of the semi-elliptical surface flaw geometry, with the crack centered at the origin of the Cartesian coordinate system. The semi-major and semi-minor axes of the ellipse are denoted by c and a, respectively, and the points on the crack surface are described by the relations

$$\frac{x^2}{c^2} + \frac{z^2}{a^2} \leqslant 1, \quad y = \pm 0. \tag{1}$$

Similarly, the points on the crack boundary (front) are defined by the parametric relations

$$\frac{x^2}{c^2} + \frac{z^2}{a^2} = 1, \quad y = \pm 0, \quad x = c\cos\varphi, \quad z = a\sin\varphi. \tag{2}$$

The formulation of the considered problem can be expressed most conveniently using the Cartesian coordinates (x,y,z) and polar coordinates (ρ,θ,ω) in conjunction with the symmetrical form of the ellipsoidal coordinates (ϕ,ξ,ψ). The connections between these coordinate systems are known and are described in the reference by Kassir and Sih (1966).

In the Cartesian frame of reference, the components of the stress tensor are designated by $(\sigma_{xx},\sigma_{yy},\sigma_{zz},\sigma_{xy},\sigma_{yz},\sigma_{xz},)$. The local stress field can be found by introducing a local triply orthogonal system of ellipsoidal coordinates (ϕ,ξ,ψ) with its origin at an arbitrary point along the crack front (Fig. 2). The system (ϕ,ξ,ψ) forms a trihedral in such a way that the axes ϕ, ξ, ψ are always directed along the principal normal, tangential and bi-normal of the crack front. The projections of the stress tensor along these local axes are designated by $(\sigma_{\phi\phi},\sigma_{\psi\psi},\sigma_{\xi\xi},\sigma_{\phi\psi},\sigma_{\psi\xi},\sigma_{\phi\xi})$ and the modified stress tensor is then transformed from Cartesian to ellipsoidal coordinates in the following manner:

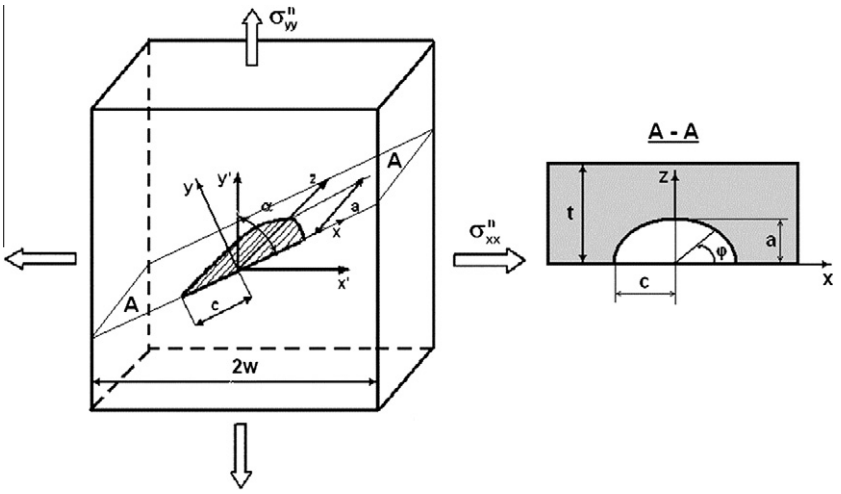

Fig. 1. A semi-elliptical inclined surface crack in a plate under remote uniform biaxial loading.

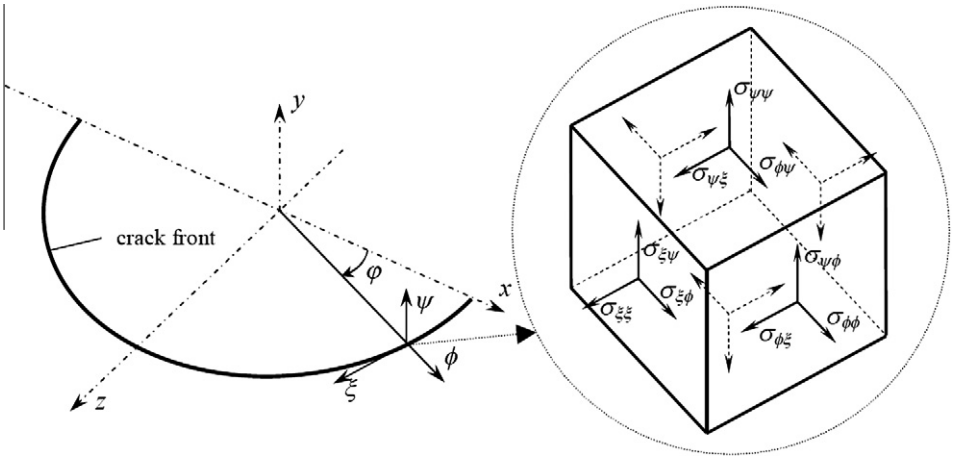

Fig. 2. Ellipsoidal coordinate system.

$$\begin{cases} \sigma_{\phi\phi} = \sigma_{xx}\cos^2\varphi + \sigma_{zz}\sin^2\varphi + 2\sigma_{zx}\sin\varphi\cos\varphi; \\ \sigma_{\psi\psi} = \sigma_{yy}; \\ \sigma_{\xi\xi} = \sigma_{zz}\cos^2\varphi + \sigma_{xx}\sin^2\varphi - 2\sigma_{zx}\sin\varphi\cos\varphi; \\ \sigma_{\phi\psi} = \sigma_{xy}\cos\varphi + \sigma_{yz}\sin\varphi; \\ \sigma_{\psi\xi} = \sigma_{yz}\cos\varphi - \sigma_{xy}\sin\varphi; \\ \sigma_{\phi\xi} = (\sigma_{zz} - \sigma_{xx})\sin\varphi\cos\varphi + \sigma_{zx}(\cos^2\varphi - \sin^2\varphi). \end{cases} \tag{3}$$

The derivation of the stress state around the contour of a semi-elliptical crack depends upon a knowledge of the limiting forms of the ellipsoidal coordinates (ϕ,ξ,ψ) and the polar coordinates (ρ,θ,ω). In Fig. 3 the stress tensor can be transformed from ellipsoidal to polar coordinates by using the expressions

$$\begin{cases} \sigma_{\rho\rho} = \sigma_{\phi\phi}\cos^2\theta + \sigma_{\psi\psi}\sin^2\theta + 2\sigma_{\phi\psi}\sin\theta\cos\theta; \\ \sigma_{\theta\theta} = \sigma_{\phi\phi}\cos^2\theta + \sigma_{\psi\psi}\sin^2\theta - 2\sigma_{\phi\psi}\sin\theta\cos\theta; \\ \sigma_{\omega\omega} = \sigma_{\xi\xi}; \\ \sigma_{\rho\theta} = (\sigma_{\psi\psi} - \sigma_{\phi\phi})\sin\theta\cos\theta + \sigma_{\phi\psi}(\cos^2\theta - \sin^2\theta); \\ \sigma_{\rho\omega} = \sigma_{\psi\varsigma}\cos\theta - \sigma_{\xi\phi}\sin\theta; \\ \sigma_{\omega\rho} = \sigma_{\psi\xi}\cos\theta + \sigma_{\xi\phi}\sin\theta. \end{cases} \tag{4}$$

2.2. Three-dimensional finite element model

Three-dimensional finite elements are used to model a plate containing a semi-elliptical surface crack. The geometry and coordinate system used are shown in Fig. 1. The finite element analyses are performed using ANSYS (1999) with twenty-node quadrilateral brick isoparametric three-dimensional solid elements. To model the 3D stress field correctly and because of the strong variations of the stress gradients, the thicknesses of the successive element layers are gradually reduced toward the free surface with respect to the crack-front line. A finite element mesh consisting of 224 elements placed along curvilinear crack front. In the circumferential direction, 40 equally sized elements are defined in the angular region from 0 to π with accordance of reference by the authors Shagivaleev and Yarullin (2005). The size of each ring increases gradually with the radial distance from the crack tip. Radial sizes of elements are varied according to the geometric progression. A finite element mesh consisting of 1,144,530 nodes and 275,784 20-node quadrilateral brick elements was used. To consider the details of a large deformation of the crack tip, a typical mesh was used to model the region near the notch tip (Fig. 4).

The FEA calculations in this work are based on the J_2 incremental theory of plasticity. The Ramberg–Osgood model

$$\frac{\varepsilon}{\varepsilon_y} = \frac{\sigma}{\sigma_y} + \alpha\left(\frac{\sigma}{\sigma_y}\right)^n \tag{5}$$

was employed to define the stress–strain curve corresponding to the elastic–plastic material properties. In Eq. (5), σ_y is the yield stress, n is the hardening coefficient and α and ε_y are the two fitting parameters. The parameter ε_y is usually taken to be equal σ_y/E. Two fitting parameters are determined by means of least squares minimization. It is well known that this fit type yields a good

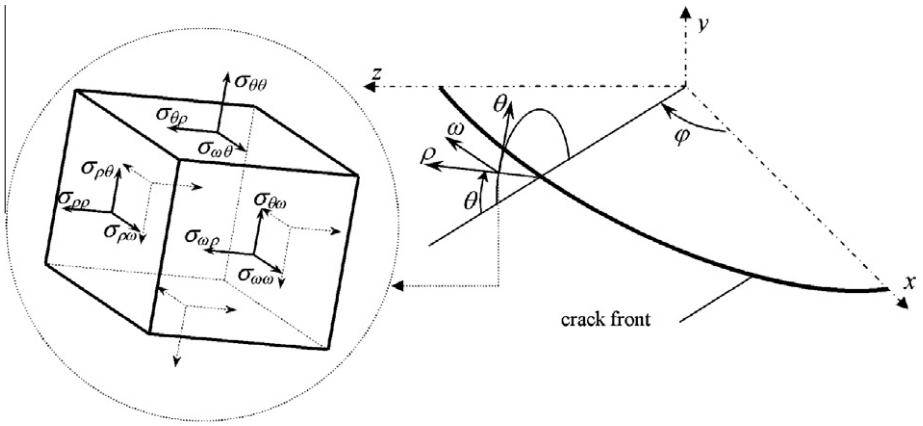

Fig. 3. Polar coordinate system.

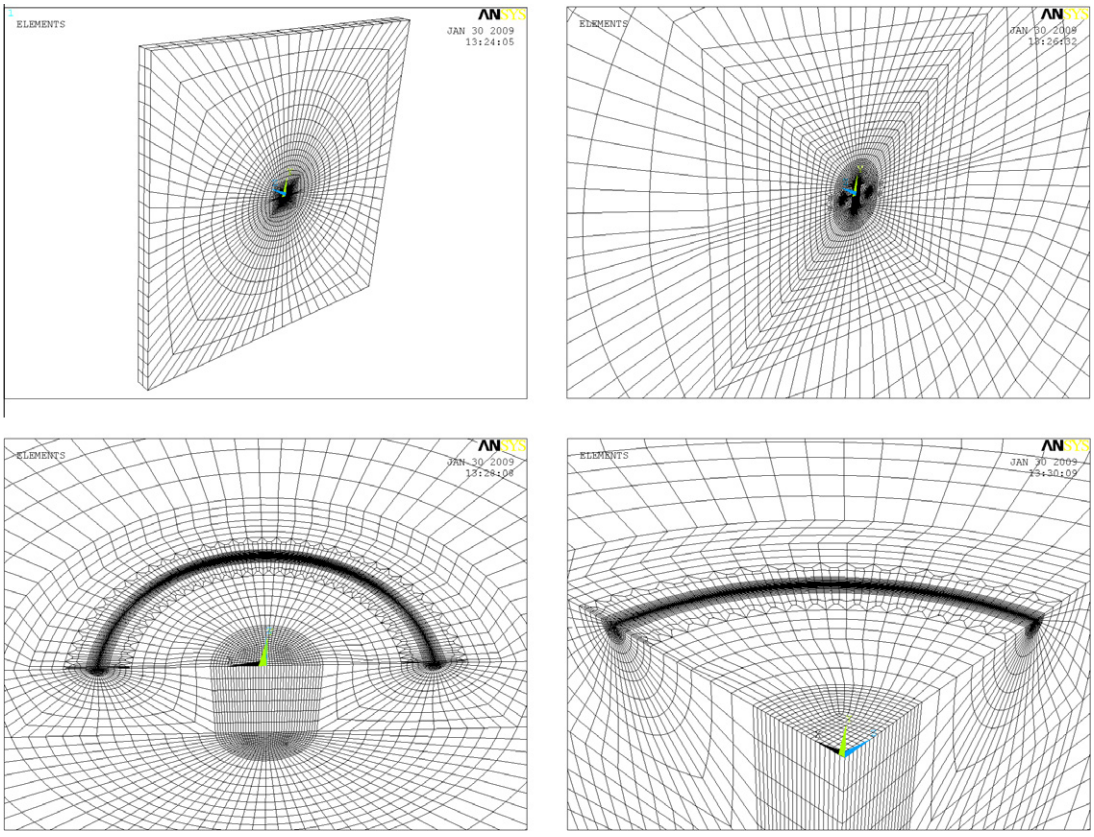

Fig. 4. Typical FE meshes of a plate containing inclined semi-elliptical surface crack.

approximation of the true stress–strain curve for high plastic strains but for low plastic strains, the stresses are lower than the experimental data. In our case, the typical relative difference between the experimental and the fitting values of the true strain is less than 5%. For all of our analyses, $\alpha = 3$, $n = 4.96$, $E = 206$ GPa, $\sigma_y = 380$ MPa, and $\nu = 0.3$ were used. To facilitate the extraction of the elastic–plastic stress field, the elastic analyses, corresponding to $n = 1$ for the geometry and loading conditions of each crack are also conducted.

The loads are applied to the far-ends of the plate (Fig. 1). The height/width ratio is fixed at 1 and the ratio a/t is fixed at 0.05 for all variants in the calculations. For all of our analyses, the (crack length)/(plate width) ratio $a/w = 0.025$ is used. The small a/t ratio is used to exclude the effect of a free boundary in the thickness direction. That is, the results of the present analyses are for plates with infinite thickness.

3. Elastic–plastic strain and stress fields

3.1. Plastic strain distributions

A review of the literature shows that, so far, the effects of the different nominal stress–strain-states are considered in the studies concerning the plastic zone at the crack tip. These effects are well known as the plane stress and the plane strain are considered. However, this does not result in an accurate estimation of the plastic zone for arbitrary three-dimensional problems because the shape and size of the plastic zone predicted by these models are different from the actual one. Our preliminary data show that, to have accurate results, the mode-mixity influence should be considered, but the effect of the crack-front position should also be taken into account. To compare the effects of different mixed modes on the resulting plastic zone at the crack tip on the free surface ($\varphi = 0$) and in the deepest point ($\varphi = \pi/2$), the following combinations of load biaxility η and crack angle α are considered (Fig. 5): equi-biaxial tension $\eta = +1$ with $\alpha = \pi/2$ and $\alpha = \pi/4$; uniaxial tension $\eta = 0$ with $\alpha = \pi/2$ and $\alpha = \pi/4$; equi-biaxial tension–compression $\eta = -1$ with $\alpha = \pi/2$ and $\alpha = \pi/4$. It should be noted that pure mode I is realized at all points of the curvilinear crack front when the crack angle equals $\alpha = \pi/2$ and for any load biaxiality.

Full-field 3D finite element analyses are carried out to determine the elastic–plastic strain and the stress fields along the curvilinear crack front in a plate subjected to different biaxial loadings. The loading level is chosen as $\sigma^{\infty}_{yy}/\sigma_{yield} = 0.425$ and the aspect ratio $a/c = 0.5$. Because of the different cases, it is difficult to present the difference between the plastic zones in a three-dimensional manner, so only two representing cuts along the crack front are shown in Fig. 5 (these are the points corresponding to $\varphi = 0$ and $\varphi = \pi/2$).

We observed that, for all examples, the size and shape of the plastic zones from finite element analyses depend on the combination of the nominal stress biaxial ratio η and the angle of crack inclination, α. A comparison of the plastic strain distributions at $\eta = +1$ for the angle of inclination $\alpha = \pi/2$ with the ones for $\alpha = \pi/4$ clearly shows that only the equi-biaxial tension is invariant with respect to the crack angle α for any point of the crack front, as is expected from an analytical consideration of a mixed-mode problem. Fig. 5 shows that, for a pure mode I ($\alpha = \pi/2$) and for any load biaxiality semi-elliptical crack, the plastic zone has a symmetrical shape with respect to the line $\theta = 0$ for both considered crack-front points.

It follows from Fig. 5 that, under the uniaxial tension with $\eta = 0$ on the free surface of plate ($\varphi = 0$) at the crack inclination angle $\alpha = \pi/4$, the plastic zone, due to the mode mixity, is non-symmetrical with respect to the initial crack plane. However, for the same

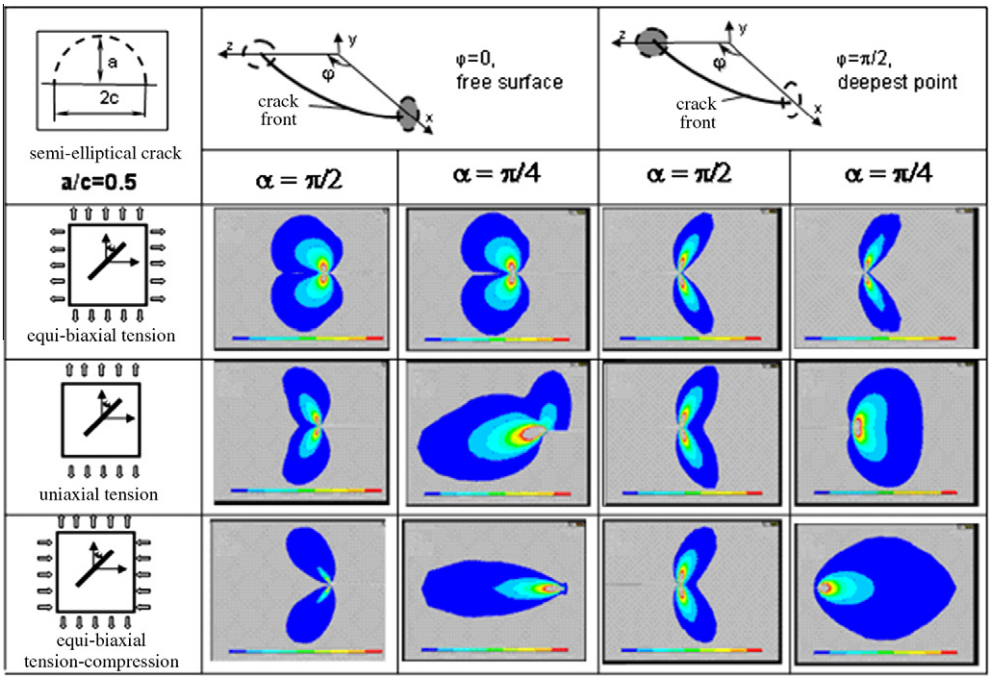

Fig. 5. Plastic zone under different biaxial loading for main crack front points.

$\eta = 0$ and $\alpha = \pi/4$ at $\phi = \pi/2$ in the deepest point of the crack front, the plastic strain distribution has a symmetrical shape. Moreover, in the deepest point of the crack front at $\alpha = \pi/4$ under the equi-biaxial tension $\eta = +1$, pure mode I is realized, whereas under the equi-biaxial tension–compression $\eta = -1$, the pure mode III takes place. A comparison of the results due to the different mode mixities we considered demonstrates that the plastic zone shows a symmetrical shape in the deepest point of the crack front. This observed plastic zone behavior can be explained by an analysis of the individual dimensionless stress component distributions.

3.2. Stress fields along the crack front

The three-dimensional finite element data have been used to determine the elastic–plastic stress component angular distributions along the surface crack front for different load bixialities. Some results for both semi-circular ($\varepsilon = 1.0$) and semi-elliptical ($\varepsilon = 0.5$) surface cracks which were subjected to remote equi-biaxial tension ($\eta = +1, \alpha = \pi/2$) and equi-biaxial tension–compression loading ($\eta = -1, \alpha = \pi/4$), are given in Fig. 6; they have dimensionless hoop stress $\tilde{\sigma}_{\theta\theta}$ and both in-plane $\tilde{\sigma}_{\rho\theta}$ and out-of-plane $\tilde{\sigma}_{\theta\omega}$ shear stresses. Remarkably, all angular stress distributions are symmetrical with respect to the crack plane $\theta = 0°$under the considered loading conditions. The results for the elastic–plastic material of angular stress distributions for general FEM-numerical solutions are normalized so that

$$\tilde{\sigma}^{FEM}_{e,\max} = \left(\frac{3}{2} s^{FEM}_{ij} s^{FEM}_{ij}\right)^{1/2}_{\max} = 1. \tag{6}$$

In Eq. (6) $\tilde{\sigma}_e$ is the Mises effective dimensionless stress and S_{ij} are the components of the deviatoric stress tensor. As can be seen from Fig. 6, both mode I hoop stress $\tilde{\sigma}_{\theta\theta}$ and mode III out-of-plane shear stress $\tilde{\sigma}_{\theta\omega}$ increase along the surface semi-elliptical crack front when the angle is altered from $\bar{\varphi} = 0$ (the free surface) to $\bar{\varphi} = 1.0$ (the deepest point). The elastic–plastic dimensionless mode II in-plane stress $\tilde{\sigma}_{\rho\theta}$ decreases due to the out-of-plane effect, and it equals zero as the deepest point is approached along the crack front. The effect of the corner singularity on all full field stress components is also evident in Fig. 6. Nevertheless, the free surface fields ($\varphi = 0$) are distinctly different from the two-dimensional plane stress field, which is due to the significance of the strong out-of-plane stress gradients.

The dimensionless angular stress component distributions are given in Fig. 7as functions of the crack inclination angle ($2\alpha/\pi$) for the semi-elliptical ($\varepsilon = 0.5$) surface crack, which is subjected to remote equi-biaxial tension–compression loading ($\eta = -1$). This loading variant was selected because particular cases contain the pure mode I ($\alpha = \pi/2$), pure mode II ($\alpha = \pi/4, \varphi = 0$) and pure mode III ($\alpha = \pi/4, \varphi = \pi/2$) at the surface semi-elliptical crack. Note that the angular stress distributions for the dimensionless crack tip distance $r/l = 0.01$ (where $l = 5$ mm) are given in Fig. 7. Additionally, equi-biaxial tensile-compression loading is analyzed at a large number of different values of inclination of the angle α. Although the loads acting at the ends of the plate are uniform tensile-compression pressure loads, the problems exhibit mixed-mode fracture conditions due to different values of the inclination angle. The elastic–plastic stress fields on the free surface shown in Fig. 7(a)–(c) may be compared to the stress fields in the deepest point of the crack front, as shown in Fig. 7(d)–(f).

Fig. 7(a) shows that, for the semi-elliptical surface flaw geometry ($\varepsilon = 0.5$) and on the free surface under equi-biaxial tension–compression loading ($\eta = -1$), the angular hoop stress distribution takes its maximum value at $2\alpha/\pi = 1$ in the crack plane at the polar angle $\theta = 0°$. It also decreases towards an inclination angle value of $2\alpha/\pi = 0.5$. After having moved from the pure mode I $2\alpha/\pi = 1$ a symmetrical-type distribution of the hoop stress because of a decreasing inclination angle α, the angular stress field at $2\alpha/\pi = 0.5$ reaches an anti-symmetrical type that corresponds to the pure mode II for a given parametrical angle of ellipse $\varphi = 0°$. Unlike this situation, in the deepest point of the crack front $\varphi = \pi/2$, the hoop stress distribution in Fig. 7(d) preserved a tendency to return to a symmetrical type because it decreased its maximum value's magnitude and, finally, $\tilde{\sigma}_{\theta\theta}$ equaled zero for any θ at $2\alpha/\pi = 0.5$.

Contrary to that behavior, the in-plane shear stress $\tilde{\sigma}_{\rho\theta}$ in Fig. 7(b) on the free surface changed from an anti-symmetrical type at $2\alpha/\pi = 1$with decreases of the crack inclination angle to a

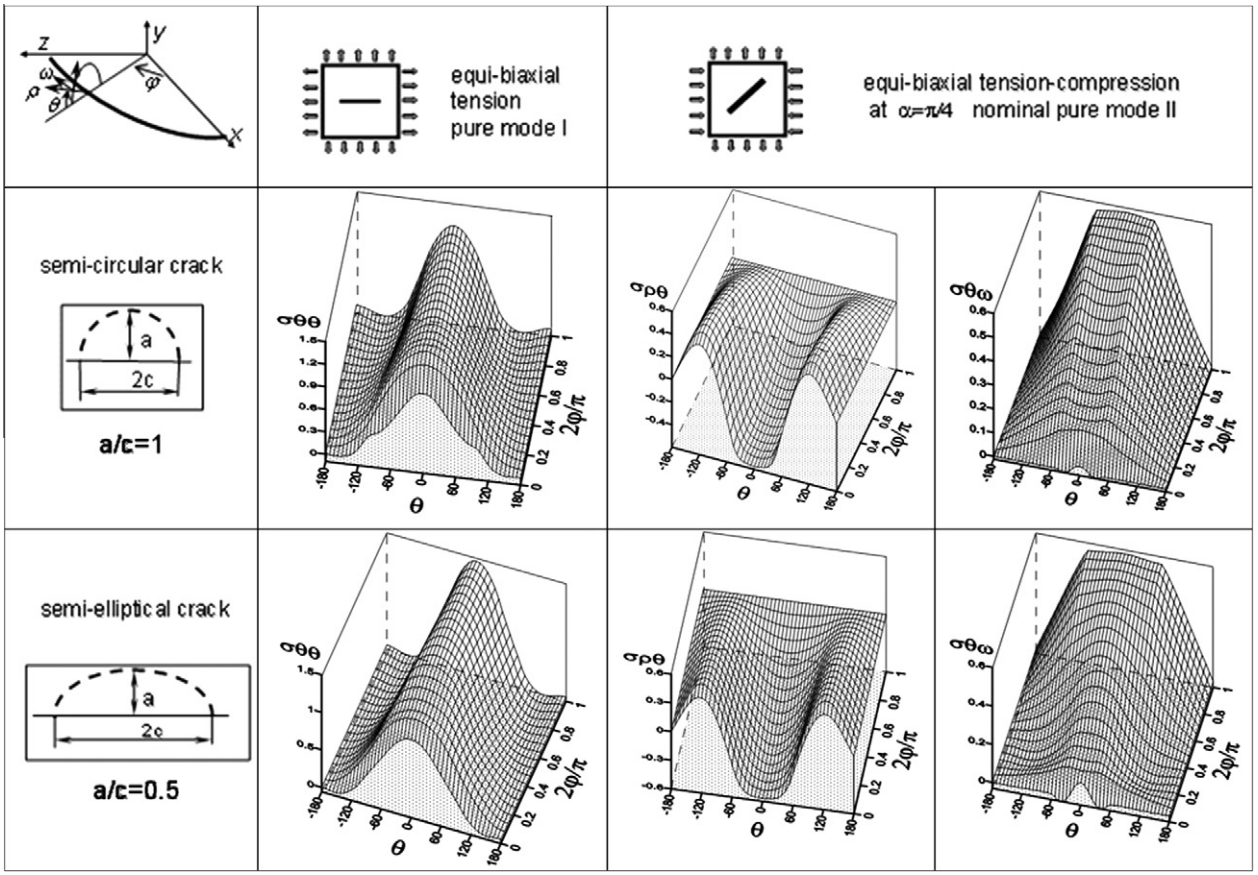

Fig. 6. Angular stress distributions along crack front of semi-circular and semi-elliptical cracks.

symmetrical distribution with respect to the crack plane $\theta = 0^\circ$ for $2\alpha/\pi = 0.5$. In the deepest point of the crack front, as shown in Fig. 7(e), the in-plane shear stress $\tilde{\sigma}_{\rho\theta}$ decreases as the inclination angle decreases, and it equals zero for any θ at $2\alpha/\pi = 0.5$. Qualitatively similar behavior of both the hoop and the in-plane shear stresses on the free surface of the plate with a semi-elliptical crack was mentioned by Shlyannikov (2003) for through-thickness mixed cracks.

On the free surface of the plate at $\varphi = 0$ when $\eta = -1$, $2\alpha/\pi = 0.5$ takes place in the mixed mode II + III, while for the same values of $\eta = -1$ and $2\alpha/\pi = 0.5$ in the deepest point of the crack front at $\varphi = \pi/2$, the pure mode III conditions are realized. This is because both the hoop stress and the in-plane shear stress are equal to zero, but the out-of-plane shear stress takes its maximum value with a symmetrical type of angular distribution, as follows from Fig. 7(f).

4. Crack-tip singularity

Under general elastic stressing, the stress field along the interior points of the crack front is the superposition of the conventional modes I, II and III, which are characterized by an inverse square root dependence on the distance from the tip. At the point where the crack front intersects the free surface, a three-dimensional corner singularity exists and its effect on the mode I, II and III stress intensity factor distributions is apparent. The relationship between the corner and interior singularity strength has been examined for specific three-dimensional, mode I (Nakamura and Parks, 1988) and mode II/III (He and Hutchinson, 2000) problems. However, only a few attempts have been made to incorporate the corner singularity in the representation of the numerical results for the surface semi-elliptical crack stress distributions.

Despite numerous elastic–plastic finite element analyses accounting for higher-order terms in stress expansion, the general understanding of both physical and mechanical fracture phenomena of 3D-mixed-mode surface flaws is far from complete. Only for two particular cases of pure mode I and pure mode II have the values of the crack tip distance exponent been proposed in the literature. Moreover, known solutions for the higher-order term amplitude factors accounting for corner effects do not have a systematic order. Therefore, only three elastic particular mixed mode cases of the crack tip singularity determination, based on the apparent stress intensity factors for surface cracks, are considered. We analyzed such far field mixed-mode loading conditions when the non-singular T-stress is equal to zero, i.e., when the first term in the elastic stress expansion is under equi-biaxial tension ($\eta = +1$) and equi-biaxial tension–compression ($\eta = -1$) with the crack inclination angle $\alpha = \pi/4$ (Williams, 1957).

We consider and use the following stress expansion in the form of equations of Eftis and Subramonian (1978):

$$\sigma_{ij} = K_i r^{\lambda} \tilde{\sigma}_{ij}^{REF}(\theta) + T\delta_{1i}\delta_{1j}, \tag{7}$$

where

$$T = \sigma_{yy}^{n}(1-\eta)\cos 2\alpha. \tag{8}$$

In Eqs. (7) and (8), r and θ correspond to the local polar coordinates measured from the periphery of the crack front in the plane perpendicular to it (Fig. 1). Also $\tilde{\sigma}_{ij}^{REF}(\theta)$ are the well known dimensionless angular stress functions, σ_{yy}^{n} is the nominal stress in the y-axis direction,$\eta = \sigma_{xx}^{n}/\sigma_{yy}^{n}$ is the nominal stress biaxial ratio and α is the inclined crack angle. The solution for arbitrary uniform remote biaxial stressing of an inclined surface crack (Fig. 1) is obtained by

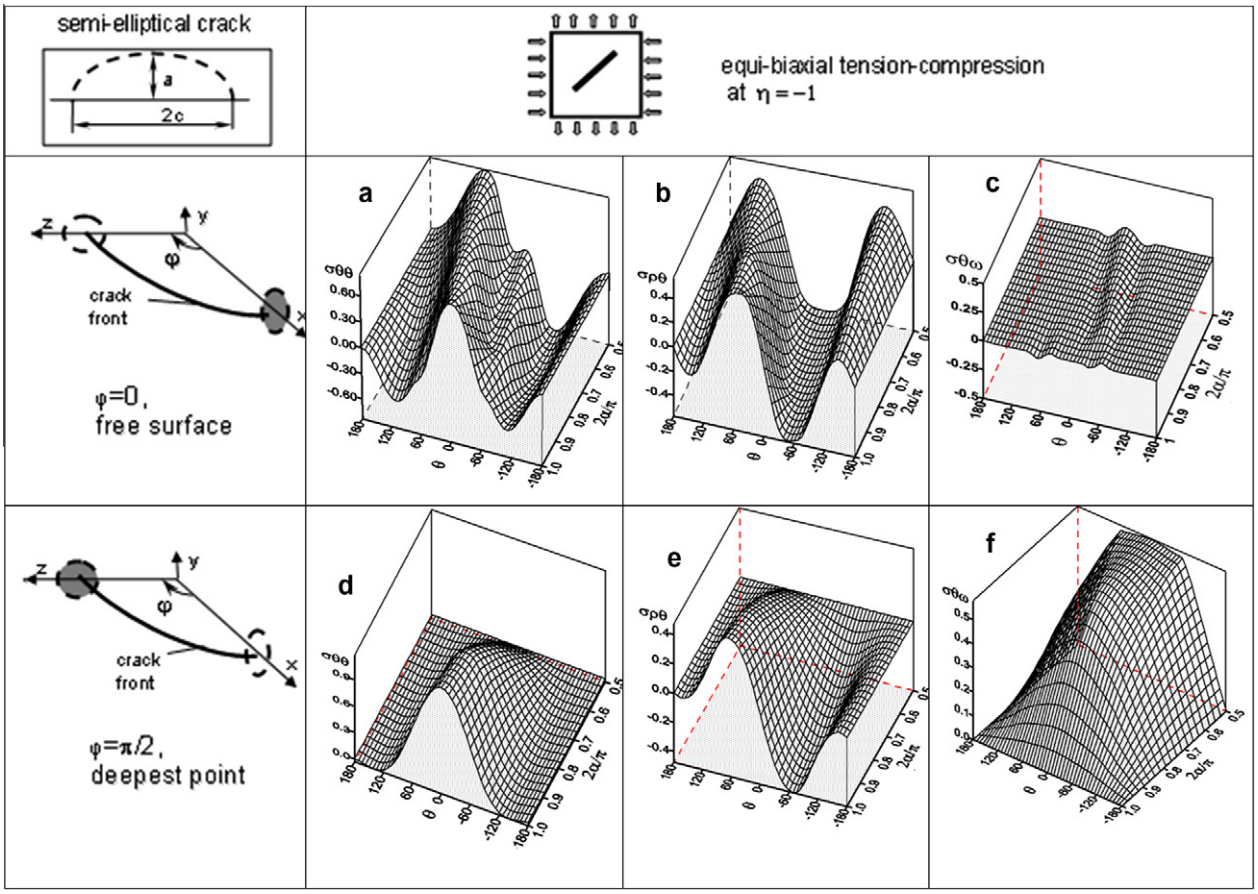

Fig. 7. Angular stress distributions as a function of crack inclination angle.

the substitution of the appropriate full field FEA stresses $\sigma_{ij} = \sigma_{ij}^{FEM}$ into Eq. (5).

The stress intensity factors for modes I, II and III of a surface semi-elliptical crack in Eq. (7) can be calculated from the general equation

$$K_i = \sigma_i^{\infty}\sqrt{\pi \cdot l}, \tag{9}$$

where l is the current crack length. This length is defined as

$$l = \frac{1}{\sqrt{\left(\frac{\cos\varphi}{c}\right)^2 + \left(\frac{\sin\varphi}{a}\right)^2}} \tag{10}$$

and the remote stresses related to the nominal biaxial stress σ_{yy}^{n} are defined as

$$\sigma_I^{\infty} = \sigma_{yy}^{n}\left(\cos^2\alpha + \eta\sin^2\alpha\right), \quad \sigma_{II}^{\infty} = \sigma_{yy}^{n}\frac{1-\eta}{2}\sin 2\alpha\cos\varphi, \quad \sigma_{III}^{\infty} = \sigma_{yy}^{n}\frac{1-\eta}{4}\sin 2\alpha\sin\varphi. \tag{11}$$

4.1. A particular case of pure mode I at equi-biaxial tension (sub-problem I)

This type of far field biaxial loading is realized when $\eta = +1$ and in this case, Eq. (8) implies $T = 0$. For such a problem, the local elastic hoop stress is

$$\sigma_{\theta\theta}^{FEM} = K_I r^{\lambda}\tilde{\sigma}_{\theta\theta}^{REF}(\theta) + 0. \tag{12}$$

It is easy to show that, from Eqs. (3) and (4) on the plane $\theta = 0°$,

$$\sigma_{\theta\theta}^{FEM} = \sigma_{\phi\phi}\sin^2\theta + \sigma_{\psi\psi}\cos^2\theta - 2\sigma_{\phi\psi}\sin\theta\cos\theta = \sigma_{\psi\psi} = \sigma_{yy}. \tag{13}$$

By substituting the dimensionless angular functions at $\theta = 0°$ into Eq. (13) are found to be

$$\sigma_{\theta\theta}^{FEM} = \frac{K_1}{(2\pi r)^{\lambda_1}}\cos\frac{\theta}{2}\left[1 + \sin\frac{\theta}{2}\sin\frac{3\theta}{2}\right] + \frac{K_2}{(2\pi r)^{\lambda_1}}\sin\frac{\theta}{2}\cos\frac{\theta}{2}\cos\frac{3\theta}{2} + 0 = \frac{K_1}{(2\pi r)^{\lambda_1}}. \tag{14}$$

By solving Eq. (14) for λ_1, the following expression is resulting for the mode I crack tip singularity is found:

$$\lambda_1 = \ln(K_1/\sigma_{\theta\theta}^{FEM})/\ln(2\pi r). \tag{15}$$

4.2. A particular case of equi-biaxial tension–compression at $\alpha = 45°$ (sub-problems II and III)

This type of far field biaxial loading is realized when $\eta = -1$ and $\alpha = \pi/4$, and in this case, Eq. (8) implies $T = 0$. In an analogous way, the crack tip singularities for sub-problems II and III are derived from the local stress field:

$$\sigma_{\rho\theta}^{FEM} = (\sigma_{\psi\psi} - \sigma_{\phi\phi})\sin\theta\cos\theta + \sigma_{\phi\psi}\left(\cos^2\theta - \sin^2\theta\right) = \sigma_{\phi\psi} = \sigma_{xy}\cos\varphi + \sigma_{yz}\sin\varphi \tag{16}$$

$$\sigma_{\theta\omega}^{FEM} = \sigma_{\psi\eta}\cos\theta - \sigma_{\eta\phi}\sin\theta = \sigma_{\psi\eta} = \sigma_{yz}\cos\varphi - \sigma_{xy}\sin\varphi. \tag{17}$$

On the plane where $\theta = 0°$,

$$\sigma_{xy}=\frac{K_I}{(2\pi r)^{\lambda}}\sin\frac{\theta}{2}\cos\frac{\theta}{2}\cos\frac{3\theta}{2}+\frac{K_{II}}{(2\pi r)^{\lambda}}\cos\frac{\theta}{2}\left(1-\sin\frac{\theta}{2}\sin\frac{3\theta}{2}\right)=\frac{K_{II}}{(2\pi r)^{\lambda}}, \tag{18}$$

$$\sigma_{yz}=\frac{K_{III}}{(2\pi r)^{\lambda}}\cos\frac{\theta}{2}=\frac{K_{III}}{(2\pi r)^{\lambda}},\quad \sigma_{zx}=-\frac{K_{III}}{(2\pi r)^{\lambda}}\sin\frac{\theta}{2}=0, \tag{19}$$

$$\begin{cases}\sigma_{\rho\theta}^{FEM}=\frac{K_{II}}{(2\pi r)^{\lambda_2}}\cos\varphi+\frac{K_{III}}{(2\pi r)^{\lambda_2}}\sin\varphi,\\ \sigma_{\theta\omega}^{FEM}=\frac{K_{III}}{(2\pi r)^{\lambda_3}}\cos\varphi-\frac{K_{II}}{(2\pi r)^{\lambda_3}}\sin\varphi,\end{cases}\quad\begin{cases}(2\pi r)^{\lambda_2}=\frac{1}{\sigma_{\rho\theta}^{FEM}}(K_{II}\cos\varphi+K_{III}\sin\varphi),\\ (2\pi r)^{\lambda_3}=\frac{1}{\sigma_{\theta\omega}^{FEM}}(K_{III}\cos\varphi-K_{II}\sin\varphi),\end{cases} \tag{20}$$

and so

$$\lambda_2=\frac{\ln\left[\frac{1}{\sigma_{\rho\theta}^{FEM}}(K_{II}\cos\varphi+K_{III}\sin\varphi)\right]}{\ln(2\pi r)},$$
$$\lambda_3=\frac{\ln\left[\frac{1}{\sigma_{\theta\omega}^{FEM}}(K_{III}\cos\varphi-K_{II}\sin\varphi)\right]}{\ln(2\pi r)}. \tag{21}$$

4.3. The elastic stress intensity factors for sub-problems I, II and III

In general case the mode I, II and III stress intensity factors K_I, K_{II} and K_{III} vary along the crack front and will be regarded as functions of the angle φ defined in Fig. 1. Based on the computed three-dimensional finite element stress intensity factors, numerical results give one grounds for taking the border effects for surface cracks into account. As a particular case of the mode II and mode III stress intensity factors by He and Hutchinson (2000) the solution is proposed for arbitrary uniform remote stressing by the superposition of the stress intensity factors of the semi-elliptical surface crack as the sum of the reference intensity factors for the full elliptical crack with corrections by polynomials accounting for behavior in the vicinity of the corner. A useful reference solution is that for the similarly aligned and loaded elliptical crack on an infinite solid. The analytical work by Kassir and Sih (1966) analyzed the behavior of such an inclined, penny-shaped crack in an infinite medium under different uniform remote loading conditions. After taking load biaxiality into account and after using existing results for the mode I stress intensity factors (Murakami (1990)), the general solution for the stress intensity factors can be written as the sum of the reference intensity factors for the full elliptical crack (the analytical solutions) with corrections by polynomials accounting for behavior in the vicinity of the corner (the FEA calculations)

$$\overline{K}_I=\overline{K}_I^{REF}[1+\eta-(1-\eta)\cos 2\alpha],\quad \overline{K}_{II}=\overline{K}_{II}^{REF}+\delta_{II}\overline{K}_{II}^{REF}\big|_{\max},$$
$$\overline{K}_{III}=\overline{K}_{III}^{REF}+2\delta_{III}\overline{K}_{III}^{REF}\big|_{\max}, \tag{22}$$

where

$$\overline{K}_I^{REF}=\frac{1}{2E_s}fF;\quad \overline{K}_{II}^{REF}=\frac{k^2\varepsilon\cos\varphi}{2Bf}(1-\eta)\sin 2\alpha;$$
$$\overline{K}_{III}^{REF}=\frac{k^2(1-\nu)\sin\varphi}{4Bf}(1-\eta)\sin 2\alpha \tag{23}$$

with elliptic integrals defined by

$$E_s=\int_0^{\pi/2}\sqrt{1-k^2\sin^2\varphi}\,d\varphi,\quad D=\int_0^{\pi/2}\frac{1}{\sqrt{1-k^2\sin^2\varphi}}d\varphi,$$
$$f=\left(\sin^2\varphi+\varepsilon^2\cos^2\varphi\right)^{1/4},\quad \varepsilon=a/c,$$
$$k=\sqrt{1-\varepsilon^2},\quad B=(k^2-\nu)E_s+\nu\varepsilon^2 D,$$
$$F=(1.13-0.09\varepsilon)(1+0.1(1-\sin^2\varphi)).$$

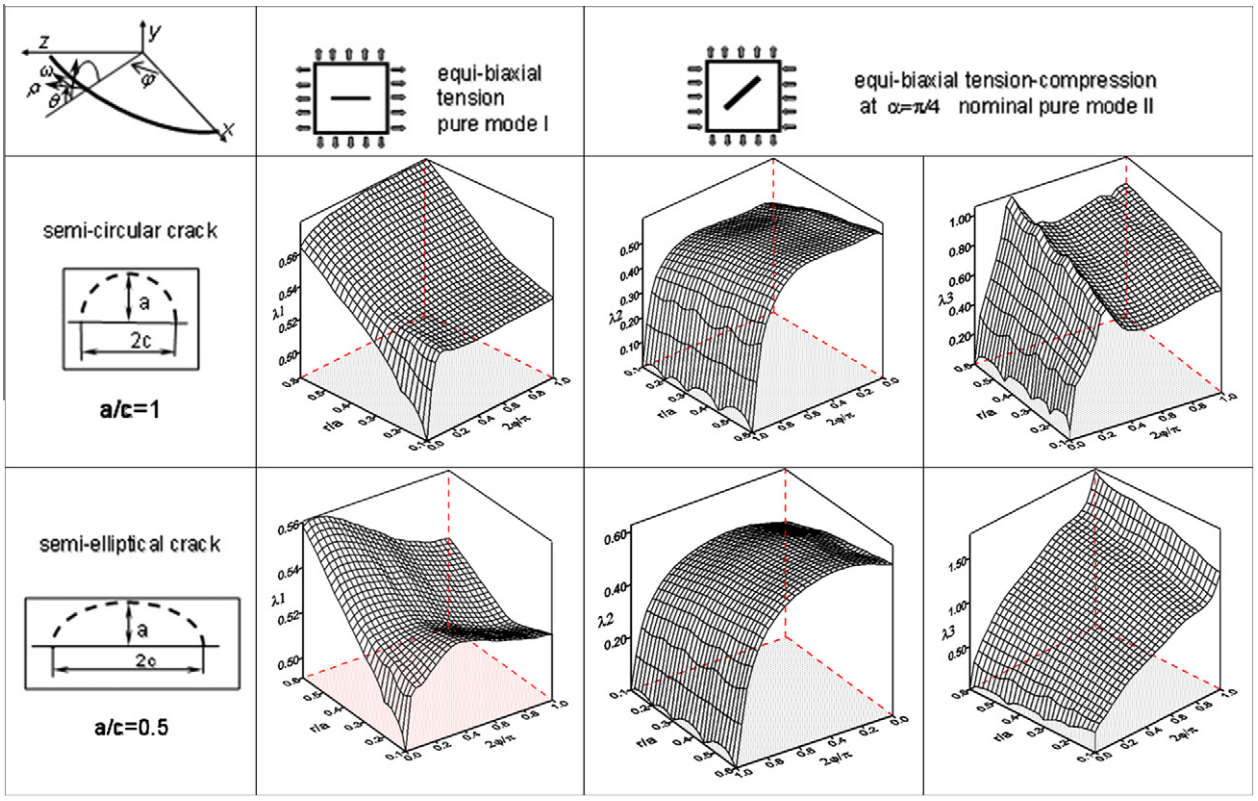

Fig. 8. Elastic crack tip singularity behavior along crack front.

The maximum values of the reference stress intensity factors will be used for scaling the surface crack solutions

$$\overline{K}_I^{REF}\big|_{\alpha=\pi/2}^{\max}=\frac{1}{E_s},\quad \overline{K}_{II}^{REF}\big|_{\varphi=0}^{\max}=\frac{k^2\sqrt{\varepsilon}}{B},\quad \overline{K}_{III}^{REF}\big|_{\varphi=\pi/2}^{\max}=\frac{k^2(1-\nu)}{2B}. \tag{24}$$

The corrections of solutions for the full elliptical crack in the infinity body are provided by polynomials accounting for different geometries in the edge of a semi-elliptical surface crack in the half-space have been given by He and Hutchinson (2000). They are based on the three-dimensional finite element results, and they are as follows:

$$\begin{aligned}\delta_{II}&=b_0+b_1\bar{\varphi}+b_2\bar{\varphi}^2+b_3\bar{\varphi}^3+b_4\bar{\varphi}^4+b_5\bar{\varphi}^5,\\ \delta_{III}&=c_0+c_1\bar{\varphi}+c_2\bar{\varphi}^2+c_3\bar{\varphi}^3+c_4\bar{\varphi}^4+c_5\bar{\varphi}^5.\end{aligned} \tag{25}$$

In Eq. (25) $\bar{\varphi}=2\varphi/\pi$ is the dimensionless angle of the semi-elliptical crack. Thus, a three-dimensional finite element results (He and Hutchinson, 2000; Murakami, 1990) and analytical solutions (Kassir and Sih, 1966) have been used to calculate the mode I, II and III stress intensity factor distributions along the surface crack front for different load biaxialities. More details for the elastic stress intensity factor calculations and distributions related to the problem considered are given by Shlyannikov et al. (2010b).

The crack tip singularity directly ahead of the crack plane at $\theta=0^\circ$ is calculated by using Eqs. (15) and (21) for the three-dimensional field in which biaxial loading is only based on the elastic stress intensity factor (when $T=0$). These singularities are shown in Fig. 8. It should be mentioned that plane stress at the free surface requires two conditions to be met, namely,

$$\sigma_{zz}=\sigma_{rz}=\sigma_{\theta z}=0,\quad \frac{d\sigma_{zz}}{dz}=\frac{d\sigma_{rz}}{dz}=\frac{d\sigma_{\theta z}}{dz}=0.$$

However the second set of equations, which requires there to be no stress gradients in the through thickness direction, is not satisfied. Under pure elastic conditions, this results in a corner field, which does not exhibit the familiar two-dimensional $r^{-1/2}$ stress singularity. This theoretical finding is confirmed by crack tip singularity distributions along the crack front in Fig. 8. Moreover, as discussed by Yusof and Hancock (2005), under perfectly-plastic conditions both the plane stress and corner fields show the familiar r^0 dependence, but the structure of the free surface field is completely different to the one in plane stresses. Compared to the in-plane shear stress distribution at the deepest point of the crack front in Fig. 7(e), the FEA results in Fig. 8 show that the crack tip singularity λ_2 is close to zero when $\bar{\sigma}_{\rho\theta}$-stress disappears at $\eta=-1$ and $\alpha=\pi/4$. This feature is also shown on the free surface by a three-dimensional field in Fig. 7(c), when the out-of-plane shear stress $\bar{\sigma}_{\theta\omega}$-stress disappears at $\eta=-1$ and $\alpha=\pi/4$ and the crack tip singularity λ_3 becomes close to zero in Fig. 8.

It follows from Fig. 8 that the effective zone of dominance of the inverse square root behavior of the crack tip singularity comprises a very small fraction of the crack front. The crack-front singularity of the mode I field λ_1 is stronger, and those of the in-plane λ_2 and out-of-plane λ_3 shear modes II and III are weaker functions of the crack tip distance, which have absolute values r that are normalized by the crack length a. Comparing the crack-front distributions for the semi-circular surface crack to the ones for the semi-elliptical crack clearly shows the influence of the surface flaw shape on the singularity behavior under different mixed modes of loading.

5. Mode-mixity parameter solutions

Following the Shih (1974) definition for the case of elasticity, the mode-mixity parameters are introduced by the following equations, which characterize the relative forces of the stress intensity factors in the far-field:

$$M_{12}^E=\frac{2}{\pi}arctg\left|\frac{\overline{K}_I}{\overline{K}_{II}}\right|,\quad M_{23}^E=\frac{2}{\pi}arctg\left|\frac{\overline{K}_{II}}{\overline{K}_{III}}\right|,\quad M_{31}^E=\frac{2}{\pi}arctg\left|\frac{\overline{K}_{III}}{\overline{K}_I}\right|. \tag{26}$$

These equations contain the elastic stress intensity factors K_I, K_{II} and K_{III} for the surface flaw, which are described by Eq. (22). With this definition of M_{ij}^E, hereby referred to as the far-field elastic mixity parameters, changes from 0 to 1, i.e., for pure mode I, $M_{12}^E=1$ and $M_{31}^E=0$; for pure mode II, $M_{12}^E=0$ and $M_{23}^E=1$; lastly, for pure mode III $M_{23}^E=0$ and $M_{31}^E=1$.

The near-field plastic mode-mixity parameters were introduced as ratios between corresponding local elastic–plastic stress components. This was done directly ahead of the crack tip at $\theta=0$ in polar coordinates (Eq. (2)) in the following form:

$$M_{12}^P=\frac{2}{\pi}arctg\left|\frac{\bar{\sigma}_{\theta\theta}}{\bar{\sigma}_{\rho\theta}}\right|,\quad M_{23}^P=\frac{2}{\pi}arctg\left|\frac{\bar{\sigma}_{\rho\theta}}{\bar{\sigma}_{\omega\theta}}\right|,\quad M_{31}^P=\frac{2}{\pi}arctg\left|\frac{\bar{\sigma}_{\omega\theta}}{\bar{\sigma}_{\theta\theta}}\right|. \tag{27}$$

The dimensionless elastic–plastic stress components $\bar{\sigma}_{ij}=\sigma_{ij}/\sigma_o$ are obtained by a full-field FEA solution. Based on the numerical results for the angular stress component distributions along the inclined surface crack front under different load biaxialities, the values of the plastic mode-mixity parameters have been determined for the semi-circular and semi-elliptical surface flaws. Thus, M_{ij}^P are defined in terms of the tensile, in-plane and out-of-plane shear stresses, where M_{ij}^P also ranges from 0 to 1, i.e., for pure mode I, $M_{12}^P=1$ and $M_{31}^P=0$; for pure mode II, $M_{12}^P=0$ and $M_{23}^P=1$; for pure mode III, $M_{23}^P=0$ and $M_{31}^P=1$. For the most general 3D elastic or plastic case of an arbitrarily shaped surface flaw, an equivalent mode-mixity parameter can be calculated from the equation

$$M=\sqrt{(M_{12})^2+(M_{23})^2+(M_{31})^2}. \tag{28}$$

As shown in Fig. 9, the mixity parameters' distributions account for all ratios between the I/II, II/III, III/I modes along the crack front of a semi-elliptical surface crack in a plate with an aspect ratio of $\varepsilon=a/c=0.5$ under far-end loads have been determined. Fig. 9(a)–(f) illustrates the elastic mode-mixity parameters' (M_{ij}^E) behavior as a function of the crack-front position φ and the inclination angle α of a semi-elliptical surface crack under biaxial tension with a ratio $\eta=0.5$ (Fig. 9(a)–(c)) and under equi-biaxial tension–compression with $\eta=-1$ (Fig. 9(d)–(f)). Shlyannikov et al. (2010a) obtained plastic mode-mixity parameter M_{ij}^P distributions, which we do not show here, for a semi-elliptical surface crack in a biaxially loaded finite thickness plate. Comparison of such distributions reveal that, under biaxial loading as a function of the crack-front location and the inclination angle in a qualitative sense, results for the elastic and plastic mode-mixity parameters' behavior show similar trends. As follows from results presented in Fig. 9, all fracture modes are encountered along the crack front when an inclined surface crack is subjected to remote uniform biaxial loading at different intensities. Both the plastic and the elastic mode-mixity parameters, like K_I/K_{II}, K_{II}/K_{III} and K_I/K_{III}, do not remain constant along the curvilinear crack front of the surface flaw.

Fig. 9(b) and (e) shows that the behavior of the elastic mixity parameter M_{23} along the crack front is invariant with respect to the initial crack angle α and the biaxial stress ratio η. Although it is not true in this situation, it is often observed that the mixity parameters M_{12} and M_{31}have a significant difference in the crack inclination angle distributions for different biaxial loading cases. Moreover, the biaxial tension case with $\eta=0.5$ is very sensitive to a change in the mode mixity in the vicinity of the free surface of a plate.

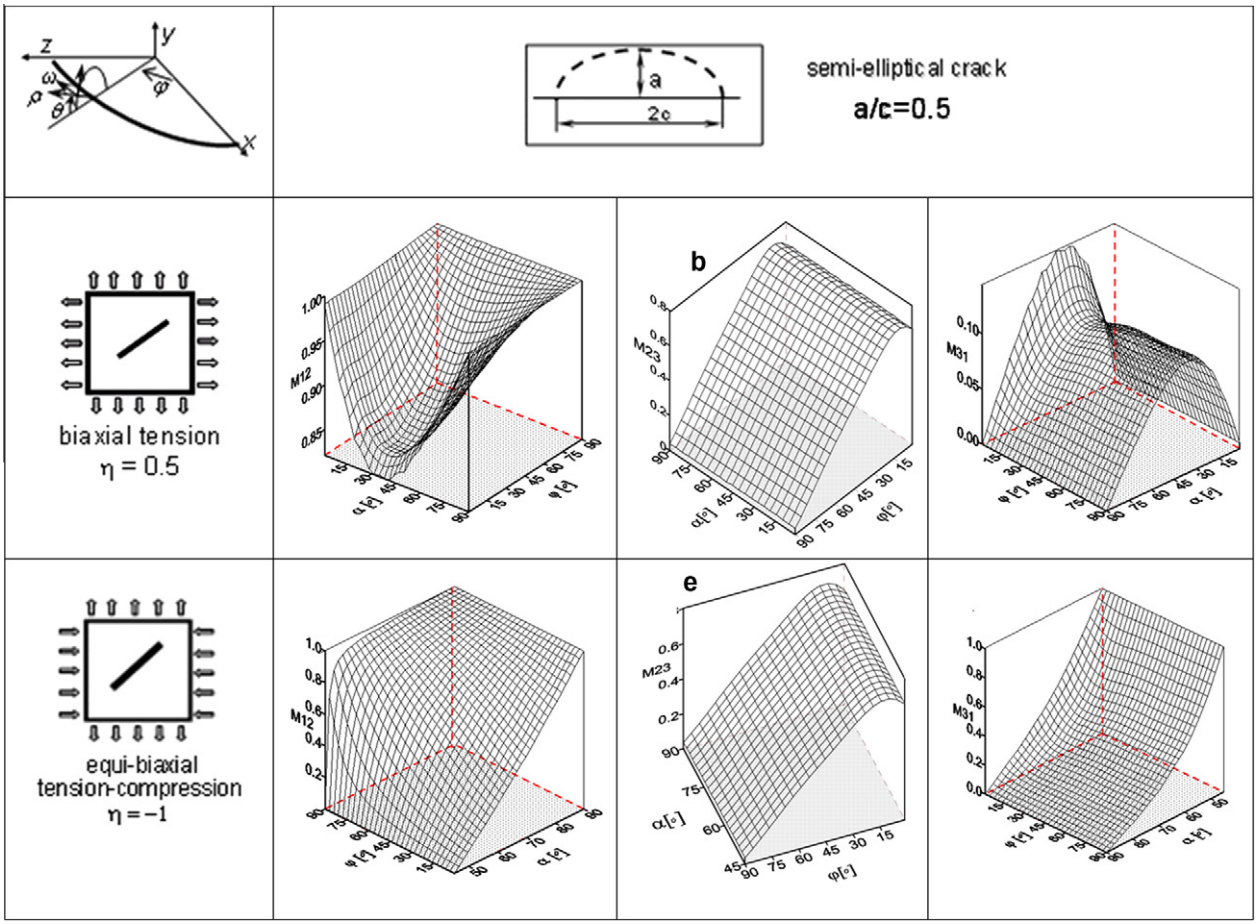

Fig. 9. Mode mixity parameters distributions along inclined crack fronts.

The plastic mode-mixity parameter (M_{ij}^{P}) distributions for different crack-front distances (r/a), including the crack-front position when (r/a) = 0 under uniaxial tension $\eta = 0$ with inclination angle $\alpha = 45°$of the semi-elliptical surface crack $\varepsilon = 0.5$, are plotted in Fig. 10. The corresponding elastic mixity parameter (M_{ij}^{E}) distributions are presented for purposes of comparison. In Fig. 10 cases 1, 2, 3 and 4 correspond to the FEA elastic–plastic solutions at different locations near the crack front ($1 - r/a = 0.0$, $2 - r/a = 0.0067$, $3 - r/a = 0.02$, $4 - r/a = 0.04$),while case 5 represent mode mixity parameters computed applying the elastic stress intensity factors K_I, K_{II} and K_{III} for the surface flaw, which are described by Eq. (22). In Fig. 10 $\bar{\varphi} = 2\varphi/\pi$ is the dimensionless angle of the semi-elliptical crack.

As can be seen from this figure, the plastic mode mixity M_{12} roughly increases along the surface semi-elliptical crack front when the angle of the free surface of the plate is altered from $\bar{\varphi} = 0$ to $\bar{\varphi} \approx 0.05$ with a dimensionless distance increasing from (r/a) = 0 to (r/a) = 0.0067. For the surface cracks M_{12}, smooth increases with respect to the crack-front angle in the range of $0.05 < \bar{\varphi} < 1$ were observed. It should be pointed out that the free-surface effect is also evident in Fig. 10 for plastic mixity parameters M_{23} and M_{31}. It is observed that, for the surface cracks in the vicinity of the corner, M_{23} displays non-uniform behavior and M_{31} does not go smoothly to 1 when $\bar{\varphi} < 0.2$, which is consistent with the existence of a corner singularity differ than $-1/(n+1)$ dependence in the HRR-solution, where n is the strain hardening exponent of the material. As it is shown in Fig. 10, the mode-mixity parameters M_{12} and M_{31} are the largest where the crack penetrates most deeply into the body $\bar{\varphi} = 1$with respect to its levels near the free surface.

It should be pointed out that Fig. 10 gives a very clear demonstration of the border's effects on both the elastic and plastic

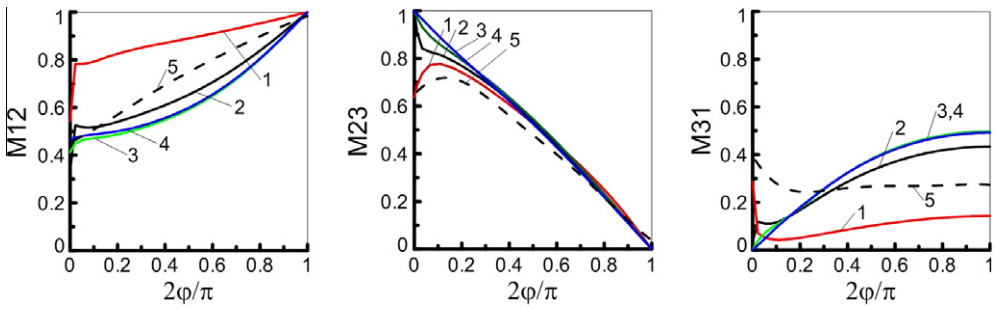

Fig. 10. Comparison mode mixity parameters distributions under uniaxial tension (1- r/a = 0.0, 2 – r/a = 0.0067, 3 – r/a = 0.02, 4 – r/a = 0.04, 5 – elastic solution).

mode-mixity behaviors at the surface crack-front position corresponding to $0° < \varphi < 10°$. Moreover, in some cases when the dimensionless crack-front distance is more than $(r/a) = 0.04$ the numerical elastic–plastic results for the mixity parameter distributions along the crack front nearly coincide with the elastic analytical solution at the deepest point of the curvilinear surface crack front.

It should be noted that, based on the full-field FEA solution, the generalized mixed-mode parameters in the form of Eq. (28) can be applied to study the competition between the dominant fracture mechanisms. It is clear that both the proposed elastic and the proposed plastic mode-mixity parameters, which are meant account for all three fracture modes' variations along an inclined surface crack under biaxial loading, are useful in the establishment of the tensile-shear transition criteria, the crack growth direction criteria and the crack path prediction for elastic–plastic materials.

6. Crack growth direction

As follows from the results presented in Figs. 9 and 10, all fracture modes are encountered along the crack front when the inclined surface crack is subjected to remote uniform biaxial loading at different intensities. Due to the mode-mixity parameters' changes along the crack front, the crack growth direction angles must also change from point to point along the crack front. This leads to different degrees of non-planar extension along the crack front.

A literature review shows that, so far, in the studies concerning the crack growth direction, the two most popular fracture criteria are the maximum tangential stress (MTS) criterion and the strain energy density (SED) criterion. They were first proposed by Erdogan and Sih (1963) and Sih (1974), respectively. The MTS criterion states that a crack will initiate in the direction θ^*, where the largest circumferential stress at a small distance from the crack tip reaches a critical value, where

$$\frac{\partial \sigma_{\theta\theta}}{\partial \theta}|_{r=r_C} = 0, \quad \frac{\partial^2 \sigma_{\theta\theta}}{\partial \theta^2}|_{r=r_C} < 0. \tag{29}$$

In the present study, crack propagation angles are determined by applying the MTS criterion along the crack front for inclined surface cracks in a straightforward manner. The solution uses a stress components transformation from the Cartesian frame to the ellipsoidal-polar coordinate system, in accordance with Eqs. (3) and (4), to find, on the base of full-field FEA results of the angular tangential stress, $\sigma_{\theta\theta}^{FEM}(\theta)$-distributions along the crack front. These distributions then allow for the prediction of a crack's growth direction in a 3D case. It is easy to show from Eqs. (3) and (4) that

$$\sigma_{\theta\theta}^{FEM} = \sigma_{\phi\phi} \sin^2\theta + \sigma_{\psi\psi} \cos^2\theta - 2\sigma_{\phi\psi} \sin\theta \cos\theta, \tag{30}$$

where

$$\sigma_{\phi\phi} = \sigma_{xx} \cos^2\varphi + \sigma_{zz} \sin^2\varphi + 2\sigma_{zx} \sin\varphi \cos\varphi; \quad \sigma_{\psi\psi} = \sigma_{yy},$$
$$\sigma_{\phi\psi} = \sigma_{xy} \cos\varphi + \sigma_{yz} \sin\varphi.$$

The strain energy density criterion was introduced by Sih (1974), and it is based on the assumption that a continuum may be presented as an assembly of small elements, each of them containing a unit volume of solid that can store a finite amount of energy at a given instance of time. The energy per unit volume was called the strain energy density function dW/dV. The theory is than applied to a number of problems of brittle and ductile static, cyclic and dynamic fracture (Sih, 1974; Shlyannikov, 2003; Shlyannikov et al., 2010b). The SED theory predicts failure by fracture and/or yielding, and it is based on the following hypotheses:

- the location of fracture initiation is assumed to coincide with the maximum or minimum of (dW/dV) or $(dW/dV)_{\min}^{\max}$;
- a fracture initiate at the location where $(dW/dV)_{\min}^{\max}$ reaches a critical value $(dW/dV)_c$ is a characteristics of the material;
- once a crack is extended after reaching $(dW/dV)_c$, it can be propagate stably. Therefore, the SED can be determined by the following expression

$$\left(\frac{dW}{dV}\right)_C = \frac{S_C}{r_C}, \tag{31}$$

where $(dW/dV)_c$ is the area under the true stress and strain curve, while r_c is the distance from the tip to the point where global instability starts. For elastic–plastic materials' behavior, the strain energy density function dW/dV can be written as

$$\frac{dW}{dV} = \frac{\sigma_o^2}{E}\left[\frac{1+\nu}{3}\bar{\sigma}_e^2 + \frac{1-2\nu}{6}\bar{\sigma}_m^2 + \frac{\bar{\alpha}n}{n+1}\bar{\sigma}_e^{n+1}\right]$$
$$\bar{\sigma}_m = \frac{\sigma_m}{\sigma_o} = \frac{1}{3\sigma_o}(\sigma_{xx} + \sigma_{yy} + \sigma_{zz}), \quad \bar{\sigma}_e = \frac{\sigma_e}{\sigma_o} = \frac{1}{\sigma_o}\left(\frac{3}{2}s_{ij}s_{ij}\right)^{1/2}, \tag{32}$$

where σ_e and s_{ij} are the equivalent and deviatoric stresses, respectively.

In the present work, the third hypothesis of the SED-criterion is used to determine the angle of crack propagation θ^*. Thus, a line drawn from each point on the crack front in the normal plane at the angle θ^* with respect to the crack plane indicates the directions in which the strain energy density has its minimal value, which is where

$$\left.\frac{\partial \overline{W}}{\partial \theta}\right|_{r=r_C} = 0, \quad \left.\frac{\partial^2 \overline{W}}{\partial \theta^2}\right|_{r=r_C} > 0, \quad \overline{W} = dW/dV. \tag{33}$$

Again, the full-field FEA angular stress component distributions $\sigma_{ij}^{FEM}(\theta)$ were used to directly calculate the SED values under different biaxial loading conditions.

The main hypotheses of the maximum tangential stress and the strain energy density theories are associated with the concept of a characteristic distance. This characteristic distance is often identified with the fracture damage zone. A critical distance ahead of the crack tip r_c, is assumed to exist when the strain energy density in an element reaches a certain critical value. For further information on the employment of the strain energy density theory, taking into account the critical distance or the fracture damage zone size for the solution of mixed-mode problems, see Shlyannikov (2003).

Finally, by substituting Eq. (30) into Eqs. (29) and (32) into Eq. (33), the values of the crack growth direction angle θ^* at all points of the crack periphery can be calculated for different combinations of load biaxiality, mode mixity and surface flaw geometry in accordance with the MTS and the SED criteria.

Using both the MTS and the SED criteria, the crack extension angles θ^* are plotted for the surface flaws in Fig. 11 as functions of both inclination and crack-front position angles for different biaxial loading conditions of semi-elliptical ($\varepsilon = 0.5$) cracks. We state three different biaxial loading conditions, which we considered to be particular cases of general biaxial stress: equi-biaxial tension–compression ($\eta = -1$), biaxial tension ($\eta = 0.5$) and uniaxial tension ($\eta = 0$). Each type of biaxial loading is analyzed at a large number of different values of the inclination angle α. Fig. 11 shows the behavior of the crack growth direction angle θ^* along the surface crack front for a dimensionless crack tip distance $r/l = 0.01$. As shown in Fig. 1, the crack-front position angle φ is measured from the free surface $\varphi = 0°$ and it equals $\varphi = 90°$ at the deepest point of the crack front.

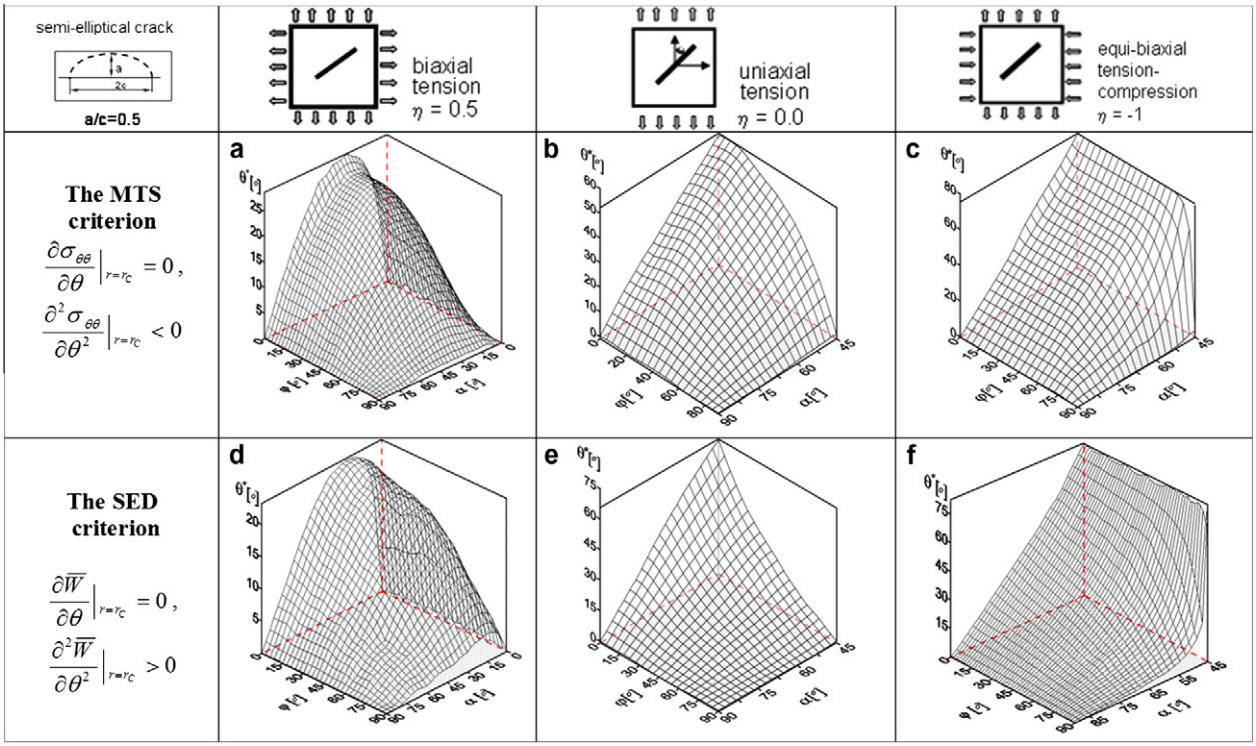

Fig. 11. Crack propagation angles along inclined crack fronts at $r/l = 0.01$.

Comparing Fig. 11(a)–(c) with Fig. 11(d)–(f) reveals that, for the same load biaxiality, the crack growth direction angle behavior for the MTS and the SED criteria have a moderate difference. It is observed that the crack propagation angle θ^* for inclination angle $\alpha = 45^\circ$ has a significant difference along the crack front under uniaxial tension $\eta = 0$. Another conclusion drawn from Fig. 11 is that, in the deepest point of the crack front at $\varphi = 90^\circ$ and under equi-biaxial tension–compression $\eta = -1$ for the SED criterion, the range of the crack extension angle variation as a function of the crack inclination angle becomes bigger relative to the MTS criterion. Nevertheless, both crack growth direction criteria have shown a similar trend for a given load biaxiality, which depends on the crack-front position and the surface flaw inclination. The presented numerical results for the strain energy density criterion are in good agreement with the recent analytical findings by Shlyannikov et al. (2010b).

It can also be observed from Fig. 11(c) and (f) that, for the semi-elliptical surface flaw geometry ($\varepsilon = 0.5$), under equi-biaxial tension–compression loading ($\eta = -1$), the crack growth angle θ^* takes its maximum value near the free surface and a nearly constant value along most part of the crack front then decreases towards the deepest point. It should be noted that, on the free surface of plate at $\varphi = 0^\circ$ when $\eta = -1$, $\alpha = 45^\circ$ realized the mixed mode II + III and the crack propagation angle is equal to θ^*=75–79°, while for the same values of $\eta = -1$, $\alpha \approx 45^\circ$ near the deepest point of the crack front $\varphi = 90^\circ$, so the crack extension angle experiences a sudden jump to $\theta^* \approx 1$–10°. Unlike in this situation, under uniaxial tension ($\eta = 0$), the crack growth angle θ^* moderately decreases along the semi-elliptical crack front towards the deepest point. As can be seen in Fig. 11(b) and (e), it depends on the given inclination angle.

As shown in Fig. 11(a) and (d), biaxial tension with a ratio of $\eta = 0.5$ is a special case of the obtained solution. When moving

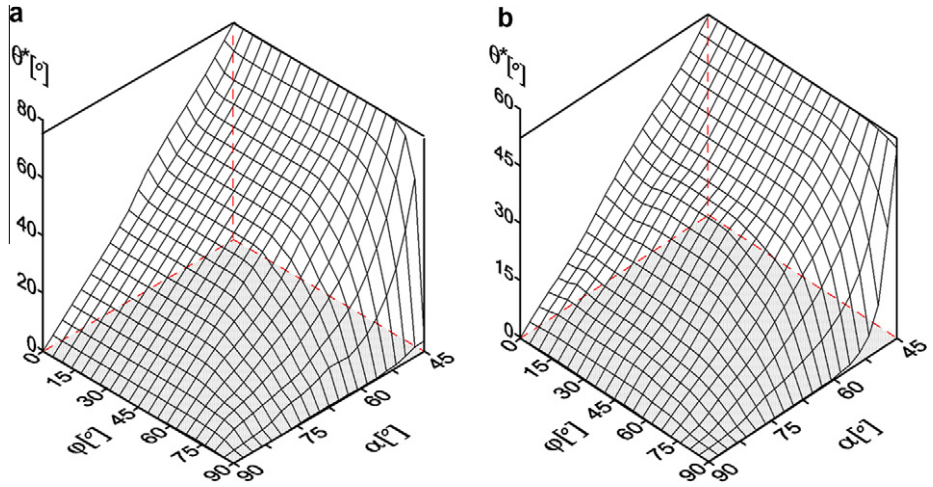

Fig. 12. Crack propagation angles along inclined crack fronts at (a) $r/l = 0.01$ and (b) $r/l = 0.06$.

from the pure mode I $\alpha = 90^\circ$ with a decreasing inclination angle α, the crack propagation angle θ^* increases until $\alpha \approx 20^\circ$, where it reaches its maximum value in magnitude for a given parametrical angle of ellipse $\varphi = 0^\circ$. Then, θ^* decreases as the inclination angle decreases and, finally, θ^* reaches $\theta^* = 0^\circ$ at $\alpha = 0^\circ$, which again corresponds to the pure mode I. The same tendency is observed at other given values of φ. Similar behavior, in a qualitative sense, on the free surface of a plate with a semi-elliptical crack was observed experimentally by Shlyannikov (2003) for a through-thickness mixed crack in biaxially loaded thin specimens.

Fig. 12 shows the behavior of the crack growth direction angle θ^* for the different crack tip distance along the whole crack front, i.e., $r/l = 0.01$ and $r/l = 0.06$. The results are presented for the MTS criterion under equi-biaxial tension–compression loading $\eta = -1$ of a semi-elliptical ($\varepsilon = 0.5$) surface crack. It is observed that, as the crack tip distance increases from $r/l = 0.01$ to $r/l = 0.06$, the crack propagation angle θ^*decreases slightly along the crack front as a function of the crack inclination angle. It should be pointed out that Fig. 12 gives a very clear demonstration of the necessity of taking into account the critical distance r_c ahead of the crack tip's effect on the behavior of the crack growth angle θ^*, which is done by applying different fracture criteria. Thus, the obtained solution for the crack growth direction criterion is sensitive to the fracture process zone size's effect, due to corresponding values of the critical distance.

7. Conclusions

Numerical solutions for predicting the parameters which describe a 3D surface crack's behavior under mixed-mode biaxial loading are presented in this paper. For a wide range of crack inclination angles, elastic–plastic stress fields along the crack front for both semi-circular and semi-elliptical surface cracks being subjected to remote biaxial loading have been obtained. For both crack geometry types, it was demonstrated that, in the vicinity of the corner, the behavior stress fields differ from the stress component distributions at the deepest point on the crack front. This phenomenon is due to the free surface effect. Using the von Mises yield criterion, the influences of the load biaxiality, crack-front position and crack inclination angle on the size and shape of the plastic zone are discussed. Combining analytical solutions and 3D finite element calculations, the elastic crack tip singularity for a surface semi-elliptical crack has been investigated on a biaxially loaded plate. The distributions of singularity exponents have been obtained along the crack front for three main cases of mixed-mode loading.

For several combinations of initial flaw geometry and load biaxiality, elastic–plastic stresses are calculated numerically to determine the mode-mixity parameters. The influence of aspect ratio of the semi-elliptical surface flaw, the biaxial loading and the initial crack angle on both elastic and plastic mode-mixity parameters distributions are discussed. In all situations, it is found that the behavior of mixed-mode parameters along a curvilinear crack front strongly depends on the crack-front position described by the parametrical semi-ellipse angle. In the particularly case of a pure shear nominal stress state, the mode-mixity parameters changed from pure mode II near the border of the semi-elliptical surface crack to pure mode III at the deepest point of crack front.

The computational data for the surface flaw elastic–plastic stress fields are used for the MTS and the SED criteria determination, and they allow for the calculation of the crack growth's direction for a 3D case of surface flaw biaxial loading. It was shown for both semi-circular and semi-elliptical crack types that the load biaxiality has a principal effect on the crack growth direction angle's behavior along the crack front.

Acknowledgments

The authors gratefully acknowledge the financial support of the Federal Agency on Science and Innovation of Russia under the Project 02.740.11.0205.

References

ANSYS, 1999. Structural Analysis Guide. 001245. Fifth ed. SAS IP, Inc.
Aoki, S., Kishimoto, K., Yoshida, T., Sakata, M., 1987. A finite element study of the near crack tip deformation of a ductile material under mixed mode loading. Journal Mechanics Physics Solids 35, 431–455.
Ayhan, A.O., 2004. Mixed mode stress intensity factors for deflected and inclined surface cracks in finite-thickness plates. Engineering Fracture Mechanics 71, 1079–1099.
Burdekin, F.M., Xu, W.G., 2003. Effects of biaxial loading and residual stresses on constraint. International Journal of Pressure Vessels and Piping 80, 755–773.
Dalle Donne C., 1999. The crack tip displacement vector approach to mixed-mode fracture. In: Miller, K.J., McDowell D.L. (Eds.), Mixed-Mode Crack Behavior. ASTM STP 1359, ASTM, Philadelphia, PA, pp. 21–40.
Eftis, J., Subramonian, N., 1978. The inclined crack under biaxial load. Engineering Fracture Mechanics 10, 43–67.
English, S.A., Arakere, N.K., Allen, P.A., 2010. J–T characterized stress fields of surface-cracked metallic liners bonded to a structural backing – I. Uniaxial tension. Engineering Fracture Mechanics 77, 170–181.
Erdogan, F., Sih, G.C., 1963. On the crack extension in plates under plane loading and transverse shear. Journal of Basic Engineering 85, 519–527.
He, M.Y., Hutchinson, J.W., 2000. Surface crack subject to mixed mode loading. Engineering Fracture Mechanics 65, 1–14.
Kassir, M.K., Sih, G.C., 1966. Three-dimensional stress distribution around an elliptical crack under arbitrary loadings. Journal of Applied Mechanics 33, 141–152.
Li, J., Zhang, X.B., Recho, N., 2004. J–M^p based criteria for bifurcation assessment of a crack in elastic–plastic materials under mixed mode I–II loading. Engineering Fracture Mechanics 71, 329–343.
Miura, N., Takahashi, Y., 2010. Evaluation of J-integral for surface cracked plates under biaxial loading using extended reference stress method. International Journal of Pressure Vessels and Piping 87, 58–65.
Murakami, Y. (Ed.), 1990. Stress Intensity Factors Handbook. Pergamon Press.
Nakamura, T., Parks, D.M., 1988. Three-dimensional elastic stress field near crack front of a thin elastic plate. Journal of Applied Mechanics 55, 805–814.
Ritchie, R.O., Knott, J.F., Rice, J.R., 1973. On the relationship between critical tensile stress and fracture toughness in mild steel. Journal Mechanics Physics Solids 21, 395–410.
Shagivaleev, R.F., Yarullin, R.R., 2005. Stress intensity factors calculation for hollow cylinder with surface semi-elliptical crack under inner pressure. Transactions of Academenergo 1, 104–108.
Shih, C.F., 1974. Small-scale yielding analysis of mixed plane strain crack problem. In: Fracture Analysis, ASTM STP 560. ASTM, Philadelphia, PA, pp. 187–210.
Shlyannikov, V.N., 2003. Elastic–Plastic Mixed-Mode Fracture Criteria and Parameters. Springer-Verlag, Berlin.
Shlyannikov, V.N., 2010. Fatigue crack path for inclined cracks and surface flaws under biaxial loading. Engineering Fracture Mechanics 77, 1772–1780.
Shlyannikov, V.N., Kislova, S.Yu., Tumanov, A.V., 2010. Mode mixity parameters accounting for semi-elliptical surface crack behavior. In: Proceedings of the 18th European Conference Fracture, Dresden, Germany, pp. 1–8.
Shlyannikov, V.N., Kislova, S.Yu., Tumanov, A.V., 2010b. Inclined semi-elliptical crack for predicting crack growth direction based on apparent stress intensity factors. Theoretical and Applied Fracture Mechanics 53, 185–193.
Sih, G.C., 1974. A three-dimensional strain energy density factor theory of crack propagation. In: Kassir, M.K., Sih, G.C. (Eds.), Mechanics of Fracture II. Noordhoof International Publishers, The Netherlands.
Tai, Y.H., Brown, M.W., Yates, J.R., 2010. A new solution for 3D crack extension based on linear elastic stress fields. In: Proceedings of the 9th International Conference on Multiaxial Fatigue and Fracture, Parma, Italy, pp. 97–105.
Wang, X., 2006. Fully plastic J-integral solutions for surface cracked plates under biaxial loading. Engineering Fracture Mechanics 73, 1581–1595.
Williams, M.L., 1957. On the stress distribution at the base of stationary crack. Journal of Applied Mechanics 24, 111–114.
Yusof, A., Hancock, J.W., 2005. In-plane and out-of-plane constraint effects in three-dimensional elastic perfectly-plastic crack tip fields. In: Proceedings of the 11th International Conference on Fracture, Turin, Italy, pp. 1–6.
Zhao, J., Guo, W., She, C., 2007. The in-plane and out-of-plane stress constraint factors and K–T–T_z description of stress field near the border of a semi-elliptical surface crack. International Journal of Fatigue 29, 435–443.